Global Biogeochemical Cycles

RESEARCH ARTICLE
10.1029/2018GB006003

Key Points:
- Mechanistic models of the export ratio integrated over various depths are developed based on the metabolic balance between photosynthesis and respiration
- Discrepancies between studies on the relationship between the export ratio and taxonomy, temperature, and productivity may be explained by a variety of factors, including the depths of integration, biomass, and surface light availability
- Seasonal variability in the export ratio in high latitudes is in great part controlled by mixed layer depth and photosynthetically active radiation

Supporting Information:
- Supporting Information S1

Correspondence to:
Z. Li,
zuchuanli@whoi.edu

Citation:
Li, Z., & Cassar, N. (2018). Theoretical considerations on factors confounding the interpretation of the oceanic carbon export ratio. *Global Biogeochemical Cycles*, *32*, 1644–1658. https://doi.org/10.1029/2018GB006003

Received 15 JUN 2018
Accepted 10 OCT 2018
Accepted article online 13 OCT 2018
Published online 20 NOV 2018

Theoretical Considerations on Factors Confounding the Interpretation of the Oceanic Carbon Export Ratio

Zuchuan Li[1,2] **and Nicolas Cassar**[1]

[1]Division of Earth and Ocean Sciences, Nicholas School of the Environment, Duke University, Durham, NC, USA, [2]Now at Woods Hole Oceanographic Institution, Woods Hole, MA, USA

Abstract The fraction of primary production exported out of the surface ocean, known as the export ratio (*ef* ratio), is often used to assess how various factors, including temperature, primary production, phytoplankton size, and community structure, affect the export efficiency of an ecosystem. To investigate possible causes for reported discrepancies in the dominant factors influencing the export efficiency, we develop a metabolism-based mechanistic model of the *ef* ratio. Consistent with earlier studies, we find based on theoretical considerations that the *ef* ratio is a negative function of temperature. We show that the *ef* ratio depends on the optical depth, defined as the physical depth times the light attenuation coefficient. As a result, varying light attenuation may confound the interpretation of *ef* ratio when measured at a fixed depth (e.g., 100 m) or at the base of the mixed layer. Finally, we decompose the contribution of individual factors on the seasonality of the *ef* ratio. Our results show that at high latitudes, the *ef* ratio at the base of mixed layer is strongly influenced by mixed layer depth and surface irradiation on seasonal time scales. Future studies should report the *ef* ratio at the base of the euphotic layer or account for the effect of varying light attenuation if measured at a different depth. Overall, our modeling study highlights the large number of factors confounding the interpretation of field observations of the *ef* ratio.

1. Introduction

The importance of relating oceanic carbon export to primary production has long been recognized. Building on Dugdale and Goering (1967) apportionment of primary production into *new* and regenerated production, Eppley and Peterson (1979) proposed to normalize new production to primary production (*f* ratio). These seminal papers prompted complementary efforts to characterize the factors influencing the *f* ratio and the ratio of organic carbon export or particulate organic carbon (POC) export to total primary production (*e* ratio and *pe* ratio, respectively; Aksnes & Wassmann, 1993; Baines et al., 1994; Betzer et al., 1984; Dunne et al., 2005; Henson et al., 2011; Laws et al., 2000; Michaels & Silver, 1988; Murray et al., 1996). Whereas the *f* ratio reflects the proportion of primary production fueled by new nutrients (or not fueled by regenerated nutrients), the *e* ratio reflects the proportion of primary production exported (i.e., which has escaped respiratory processes). In a steady state system with no change in elemental stoichiometry and no nitrification at the ocean surface, the *f* ratio and *e* ratio should be equal as export production should balance new production. Hereafter, we use the term *ef ratio* following Laws et al. (2000) to describe the ratio of new or export production.

Among other things, the *ef* ratio has been hypothesized to vary as a function of sea surface temperature (SST), net primary production (NPP), respiration, and sinking rates of particles. The negative relationship between the *ef* ratio and SST reported in some studies has been attributed to the stronger temperature dependency of respiration compared to photosynthesis (Cael & Follows, 2016; Dunne et al., 2005; Henson et al., 2011; Laws et al., 2000, 2011; Rivkin & Legendre, 2001). A positive relationship between the *ef* ratio and NPP and/or phytoplankton biomass concentration has also been reported in various regions of the world oceans (Dunne et al., 2005; Eppley & Peterson, 1979; Huang et al., 2012; Laws et al., 2011, 2000). Conversely, the sinking rate of particles is expected to vary as a function of their density and size (Alldredge & Silver, 1988), which are in turn related to the mineral content of the particles (Armstrong et al., 2002; Francois et al., 2002; Klaas & Archer, 2002), aggregation (Burd & Jackson, 2009; Passow et al., 1994), and plankton community structure (Boyd & Newton, 1995, 1999; Buesseler, 1998; Guidi et al., 2016; Michaels & Silver, 1988). These factors are often interconnected, which may explain the difficulty in identifying and quantifying the dominant factors.

For example, some plankton types are generally associated with high production (NPP) and biomass regimes, which may also influence aggregation (Jackson & Kiørboe, 2008; Passow et al., 1994).

In this vein, Britten et al. (2017) attributed to confounding factors the recent report of a lack of dependency of the carbon export efficiency on temperature in the Southern Ocean (Maiti et al., 2013). According to their *temperature-ballast* hypothesis, changes in ballasting masked the effect of temperature on the export efficiency (Britten et al., 2017; Henson et al., 2015). An inverse relation of the export efficiency on NPP in the Southern Ocean as reported by Maiti et al. (2013) also prompted various hypotheses for mechanisms, including trophic structure, grazing and fecal pellet production, bacterial activity and recycling, and dissolved organic carbon (DOC) export (Cavan et al., 2015; Laurenceau-Cornec et al., 2015; Le Moigne et al., 2016; Maiti et al., 2013). As importantly, a lack of steady state, for example, with export lagging production (Buesseler, 1998; Buesseler et al., 2009; Henson et al., 2015), would also bias estimates of the export ratio.

However, more fundamental factors, even at steady state, may also explain the large scatter in the relation of the carbon export efficiency on predictors. For example, the depth of the measurements (Boyd & Newton, 1995; Buesseler & Boyd, 2009; Palevsky & Doney, 2018), and the depth of the mixed layer in absolute terms and in relation to the depth of measurement of the *ef* ratio may also introduce noise. As stated by Buesseler (1998), "since both production and particulate export are strongly depth dependent, the relative ratio of these will depend upon the depth of integration." The net production of organic matter, also known as net community production (NCP) and which reflects the carbon export potential as presented in Li and Cassar (2017), is depth dependent because it results from the balance between photosynthesis, which decreases with depth, and respiration. Conversely, POC export is depth dependent because of remineralization and POC attenuation with depth. Such concepts are important but often overlooked when interpreting differences in *ef* ratios between ecosystems and between studies.

In this study, we explore how some of these factors may confound the interpretation of the *ef* ratio using a mechanistic model of the metabolic balance between photosynthesis and respiration. Using this model, we first compare *ef* ratios at different depths of integration (i.e., euphotic depth [1% of surface irradiance], fixed depth, and mixed layer depth [MLD]) and discuss factors regulating their relations to NPP. For example, two identical plankton communities may have diverging *ef* ratios because of differences in MLD, with shallower mixed layers leading to higher *ef* ratios. Similarly, our theoretical considerations predict that two ecosystems with differing autotrophic biomass and growth rates but equivalent NPP will display different *ef* ratios, with the greater growth rates leading to a higher *ef* ratio. Finally, we partition and examine the influence of the individual factors (i.e., MLD, surface irradiance, SST, nutrient concentration, and chlorophyll concentration) on the seasonality of the *ef* ratio at the base of mixed layer of the world's oceans.

2. Model Description

By definition, the volumetric NCP at depth z (NCP(z)) is equal to the volumetric NPP (NPP(z)) minus the volumetric heterotrophic respiration (HR(z)) (Li & Cassar, 2017):

$$\mathrm{NCP}(z) = \mathrm{NPP}(z) - \mathrm{HR}(z) = N_m \times I_m(z) \times \mu_{\max} \times C - r_{\mathrm{HR}} \times C \tag{1}$$

where C, $\mu_{\max}$, N_m, $I_m(z)$, and r_{HR} represent the phytoplankton biomass concentration and maximum growth rate, the effects of nutrient concentration and light availability on the phytoplankton growth rate, and the heterotrophic respiration rate, respectively (see Table 1 for a list of acronyms and definitions). N_m, $\mu_{\max}$, r_{HR}, and C are assumed to be homogeneous above the depth of integration. Neglecting light inhibition, N_m and $I_m(z)$ can be modeled to obey Michaelis-Menten kinetics (Dutkiewicz et al., 2001; Huisman & Weissing, 1994):

$$N_m = \frac{N}{N + k_m^N} \tag{2}$$

$$I_m(z) = \frac{I(z)}{I(z) + k_m^I} \tag{3}$$

where N and k_m^N represent the nutrient concentration and half-saturation constant, respectively, and I and k_m^I stand for the photosynthetically active radiation (PAR) level and half-saturation constant, respectively. PAR at depth z ($I(z)$) exponentially decays with depth according to the following equation:

Table 1
Model Parameters, Abbreviations, and Units

Parameter	Description	Units
MLD	Mixed layer depth	m
Z_{eu}	Euphotic depth	m
Z_z	A fixed depth	m
z	Depth	m
NPP(z)	Net primary production at depth z	mmol C·m^{-3}·day^{-1}
NPP(0,z)	Net primary production above depth z	mmol C·m^{-2}·day^{-1}
HR(z)	Heterotrophic respiration at depth z	mmol C·m^{-3}·day^{-1}
HR(0,z)	Heterotrophic respiration above depth z	mmol C·m^{-2}·day^{-1}
NCP(z)	Net community production at depth z	mmol C·m^{-3}·day^{-1}
NCP(0,z)	Net community production above depth z	mmol C·m^{-2}·day^{-1}
F	Export production	mmol C·m^{-2}·day^{-1}
ef_z, ef_{eu}, ef_{100}, ef_{ml}	ef_z is the export ratio at any depth z, which includes the specific cases of ef_z at the euphotic depth (ef_{eu}), 100 m (ef_{100}), and mixed layer depth (ef_{ml}).	unitless
N	Nutrient concentration	mmol/m^3
k_m^N	Half-saturation constant for nutrient concentration	mmol/m^3
N_m	Nutrient effect on the phytoplankton growth $N_m = \frac{N}{N+k_m^N}$	unitless
PAR	Photosynthetically active radiation	E·m^{-2}·day^{-1}
I_o	Photosynthetically active radiation just beneath water surface	E·m^{-2}·day^{-1}
$I(z)$	Photosynthetically active radiation at depth z	E·m^{-2}·day^{-1}
k_m^I	Half-saturation constant for PAR (4.1 E·m^{-2}·day^{-1}; Behrenfeld & Falkowski, 1997)	E·m^{-2}·day^{-1}
$I_m(z)$	Light effect on the phytoplankton growth at depth z, $I_m(z) = \frac{I(z)}{I(z)+k_m^I} = \frac{I_0\times e^{-K_I\times z}}{I_0\times e^{-K_I\times z}+k_m^I}$	unitless
$I_m(0,z)$	Integrated light effect on phytoplankton growth above depth z, $I_m(0,z) = -\frac{1}{K_I}\times \ln\left(\frac{I_0\times e^{-K_I\times z}+k_m^I}{I_0+k_m^I}\right)$	unitless
$\overline{I_z}$, $\overline{I_{eu}}$, $\overline{I_{100}}$, $\overline{I_{ml}}$	$\overline{I_z}$ represents the averaged effect of light availability on the phytoplankton growth rate within depth z, which includes the specific cases of $\overline{I_z}$ at the euphotic depth ($\overline{I_{eu}}$), 100 m ($\overline{I_{100}}$), and mixed layer depth ($\overline{I_{ml}}$).	unitless
μ_{max}	Maximum phytoplankton specific growth rate	day^{-1}
r_{HR}	Heterotrophic respiration specific rate	day^{-1}
K_I	Diffusion attenuation coefficient	m^{-1}
K_I(490)	Diffusion attenuation coefficient at 490 nm	m^{-1}
C	Phytoplankton biomass concentration	mmol/m^3
[Chl]	Chlorophyll *a* concentration	mg/m^3
POC	Particulate organic carbon	mg/m^3
DOC	Dissolved organic carbon	mg/m^3
T	Sea surface temperature	°C
P_t	Temperature dependence of phytoplankton growth rate (0.0663, Eppley, 1972)	°C^{-1}
B_t	Temperature dependence of heterotrophic respiration (0.08, Rivkin & Legendre, 2001; Lopez-Urrutia et al., 2006)	°C^{-1}
Δef_{ml}	Differential for ef_{ml}	unitless
ΔN	Change in N	mmol/m^3
ΔI_0	Change in I_0	E·m^{-2}·day^{-1}
ΔT	Change in T	°C
Δ[Chl]	Change in [Chl]	mmol/m^3
ΔMLD	Change in MLD	m

$$I(z) = I_0\times e^{-K_I\times z} \tag{4}$$

where I_0 and K_I represent PAR just beneath the water surface and the light attenuation coefficient, respectively. In the open ocean, K_I is modeled as an empirical function of the light attenuation coefficient at the wavelength of 490 nm (K_d(490)), which is in turn derived from the chlorophyll *a* concentration ([Chl]) (Morel et al., 2007):

$$K_I = 0.0665 + 0.874\times K_d(490) - \frac{0.00121}{K_d(490)} \tag{5a}$$

$$K_d(490) = 0.0166 + 0.0773\times [\mathrm{Chl}]^{0.6715} \tag{5b}$$

where the constant *0.0166* is the light attenuation at 490 nm due to pure seawater and the second term on

Table 2
Export Ratios at Different Depths of Integration

Depth of integration		Equation
Euphotic depth (Z_{eu})		$ef_{eu} = \frac{NCP(0,\ Z_{eu})}{NPP(0,\ Z_{eu})} = 1 - \frac{1}{I_{eu}} \times \frac{1}{N_m} \times \frac{r_{HR}}{\mu_{max}}$ (9)
Fixed depth (Z_Z)	$Z_Z > Z_{eu}$	$ef_z = \frac{NCP(0,Z_{eu})}{NPP(0,Z_{eu})} \times e^{-\frac{Z_z - Z_{eu}}{Z^*}} = ef_{eu} \times e^{-\frac{Z_z - Z_{eu}}{Z^*}}$ (14)
	$Z_Z < Z_{eu}$	$ef_z = \frac{NCP(0,Z_z)}{NPP(0,Z_z)} = 1 - \frac{1}{I_z} \times \frac{1}{N_m} \times \frac{r_{HR}}{\mu_{max}}$ (16a)
		$ef_z = \frac{NCP(0,Z_z)}{NPP(0,Z_z)} = 1 - \frac{\overline{I_{eu}}}{\overline{I_z}}(1 - ef_{eu})$ (16b)

Note. See Table 1 for acronyms.

the right-hand side of equation (5b) represents the light attenuation coefficient due to nonwater components (e.g., phytoplankton and colored dissolved organic matter). K_I and $K_d(490)$ increase with [Chl] ($\frac{dK_d(490)}{d[Chl]} > 0$, and $\frac{dK_I}{d[Chl]} > 0$).

3. Influence of the Depth of Measurements on the Export Production and Export Ratio

In order to evaluate how the depth of integration influences export production and the *ef* ratio, we derive equations describing these properties at the base of the euphotic layer and at a fixed depth (Table 2). To that end, we use equations (1)–(5) and build on the model presented in Li and Cassar (2017). For simplicity, we assume that μ_{max}, r_{HR}, N, k_m^N, k_m^I, [Chl], and C in equations (1)–(5) are well mixed or constant within the depth of integration. We also assume that the ecosystem is at steady state and thus that export production is equal to NCP and new production.

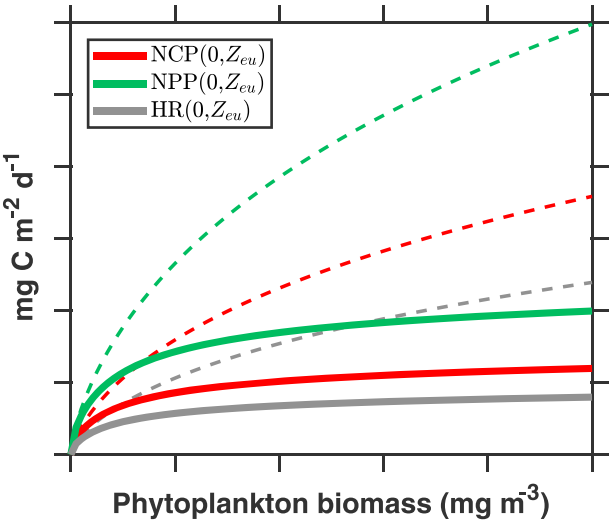

Figure 1. Schematic diagram of net community production (NCP), net primary production (NPP), and heterotrophic respiration (HR) integrated over the euphotic depth (Z_{eu}). Light attenuation coefficient (K_I) is a function of chlorophyll *a* concentration ([Chl]) (Morel et al., 2007), which is in turn modeled as a function of phytoplankton biomass concentration (C) based on the autotrophic carbon to [Chl] ratio (C : [Chl]). Dashed lines represent NCP(0, Z_{eu}), NPP(0, Z_{eu}), and HR(0, Z_{eu}) derived using a constant C : [Chl] of 90 (Arrigo et al., 2008). Solid lines represent NCP(0, Z_{eu}), NPP(0, Z_{eu}), and HR(0, Z_{eu}) with variable C : [Chl] estimated using the empirical relation between C and [Chl] derived by Jakobsen and Markager (2016).

3.1. Export Ratio at the Base of Euphotic Layer

Based on equation (1), NCP integrated over the euphotic layer (NCP(0, Z_{eu})) may be expressed as follows (Li & Cassar, 2017):

$$\begin{aligned} NCP(0,Z_{eu}) &= NPP(0,Z_{eu}) - HR(0,Z_{eu}) \\ &= \int_0^{Z_{eu}} NPP(z)dz - \int_0^{Z_{eu}} HR(z)dz \\ &= N_m \times I_m(0,Z_{eu}) \times \mu_{max} \times C - r_{HR} \times C \times Z_{eu} \end{aligned} \quad (6)$$

where NPP(0, Z_{eu}) and HR(0, Z_{eu}) represent NPP and HR integrated over the euphotic zone, respectively, Z_{eu} denotes the euphotic depth where 1% of surface PAR remains, and $I_m(0, Z_{eu})$ is calculated from equations (3) and (4) as follows:

$$I_m(0,Z_{eu}) = \int_0^{Z_{eu}} I_m(z)dz = -\frac{1}{K_I} \times \ln\left(\frac{I_0 \times e^{-K_I \times Z_{eu}} + k_m^I}{I_0 + k_m^I}\right) \quad (7)$$

where

$$Z_{eu} = -\frac{\ln(0.01)}{K_I} \quad (8)$$

The autotrophic carbon to [Chl] ratio (C : [Chl]) influences how NCP(0, Z_{eu}), NPP(0, Z_{eu}), and HR(0, Z_{eu}) respond to changes in C (Figure 1 and supporting information). Intuitively, one would expect NCP(0, Z_{eu}), NPP(0, Z_{eu}), and

$HR(0, Z_{eu})$ to monotonically increase with C, which is observed when C : [Chl] ratio is a constant. However, when accounting for the varying C : [Chl] ratio, $NCP(0, Z_{eu})$, $NPP(0, Z_{eu})$, and $HR(0, Z_{eu})$ plateau at high C. This can be explained by (1) the shoaling depth of integration Z_{eu} resulting from decreasing light availability with increasing C and [Chl] (equations (5a), (5b), and (8)) and (2) the balance between phytoplankton physiology (C : [Chl]) and the package effect on light attenuation (equation (5b)). It is worth noting that the responses of euphotic depth-integrated NCP, NPP, and HR to variations in C are markedly different from the ones presented in Figure 2 of Li and Cassar (2017), where the rates were integrated to a fixed depth (e.g., MLD) as opposed to the euphotic depth.

The export ratio at the base of the euphotic zone (ef_{eu}) can be derived from equation (6):

$$ef_{eu} = \frac{NCP(0, Z_{eu})}{NPP(0, Z_{eu})} = 1 - \frac{1}{\overline{I_{eu}}} \times \frac{1}{N_m} \times \frac{r_{HR}}{\mu_{max}} \tag{9}$$

where $\overline{I_{eu}} = \frac{I_m(0, Z_{eu})}{Z_{eu}} = \frac{1}{Z_{eu}} \times \int_0^{Z_{eu}} I_m(z) dz$ represents the averaged effect of light availability on the phytoplankton growth rate in the euphotic zone which is independent of [Chl] (equations (7) and (8)). The right-hand side of equation (9) shows that ef_{eu} is a function of the proportion of NPP not respired within the euphotic zone ($ef_{eu} = 1 - \frac{HR(0, Z_{eu})}{NPP(0, Z_{eu})}$). The μ_{max} and r_{HR} can be modeled to vary as a function of temperature (T) according to the following equations (Eppley, 1972; Lopez-Urrutia et al., 2006; Rivkin & Legendre, 2001):

$$\mu_{max} \propto e^{P_t \times T} \tag{10}$$

$$r_{HR} \propto e^{B_t \times T} \tag{11}$$

and therefore,

$$\frac{r_{HR}}{\mu_{max}} = \beta \times e^{(B_t - P_t) \times T} \tag{12}$$

where P_t and B_t represent constants and β is a parameter related to the community structure (Lopez-Urrutia et al., 2006). See Table 1 for the values attributed to these parameters.

3.2. Export Ratio at a Fixed Depth

To investigate how export production and the ef ratio at a fixed depth Z_z (ef_z) varies with Z_{eu} and [Chl], we consider the two cases when the measurement depth is deeper and shallower than the euphotic depth ($Z_z > Z_{eu}$ and $Z_z < Z_{eu}$, respectively).

3.2.1. Measurement Depth Deeper Than the Euphotic Depth

Assuming that particle flux below Z_{eu} exponentially decays with depth (Armstrong et al., 2002; Lutz et al., 2002), export production (F) when $Z_z > Z_{eu}$ can be estimated as follows:

$$F(Z_z) = F(Z_{eu}) \times e^{-\frac{Z_z - Z_{eu}}{Z^*}} \tag{13}$$

where Z^* is the remineralization length scale and $F(Z_{eu})$ is equal to $NCP(0, Z_{eu})$ at steady state. Equations (9) and (13) lead to ef_z:

$$ef_z = \frac{NCP(0, Z_{eu})}{NPP(0, Z_{eu})} \times e^{-\frac{Z_z - Z_{eu}}{Z^*}} = ef_{eu} \times e^{-\frac{Z_z - Z_{eu}}{Z^*}} \tag{14}$$

Equation (14) suggests that ef_z is smaller than ef_{eu} and increases with deepening Z_{eu} because of lower particle flux attenuation (Figure 2a). Since Z_{eu} shoals with increasing [Chl], ef_z is expected to be negatively related to [Chl]. As the depth of measurement deepens (i.e., increase Z_z), ef_z decreases because of the increasing contribution of remineralization processes. The general form of the relation between ef_z and Z_{eu} does not change if the particle attenuation in equation (14) is modeled using the Martin curve (Martin et al., 1987).

3.2.2. Measurement Depth Shallower Than the Euphotic Depth

When $Z_z < Z_{eu}$, export production and ef at Z_z may be expressed as follows:

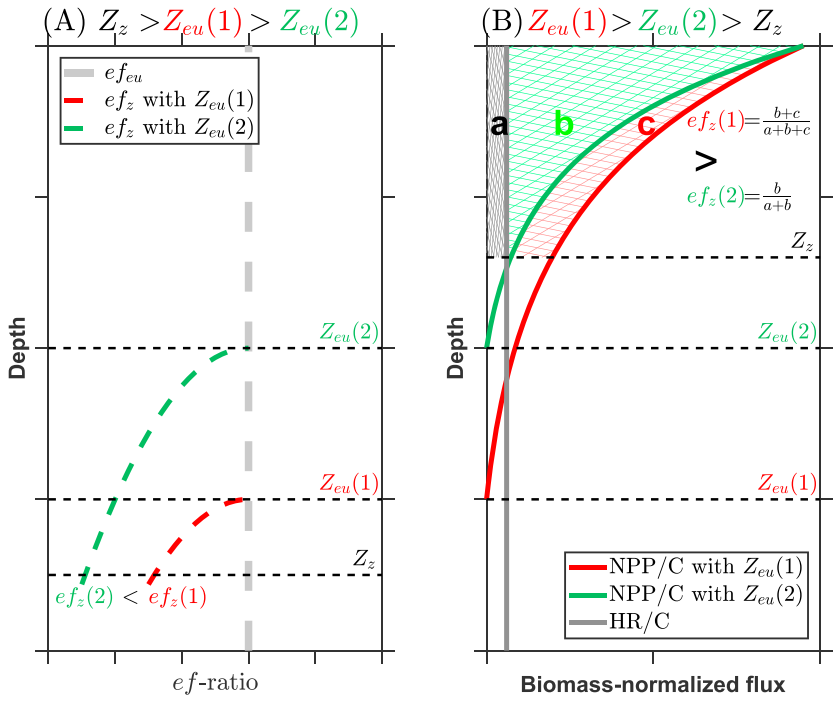

Figure 2. Schematic diagram of the export ratio as a function of the integration depth (i.e., depth horizon of measurement). (a) Case where the depth of integration Z_Z is deeper than the euphotic depths and $Z_{eu}(1) > Z_{eu}(2)$. Particles are modeled to exponentially attenuate with depth (red and green dashed curves). Because $Z_{eu}(1) > Z_{eu}(2)$, the export production with $Z_{eu}(2)$ (green dashed curve) has experienced more attenuation than the export production with $Z_{eu}(1)$ (red dashed curve) at depth Z_z. (b) Case where $Z_{eu}(1) > Z_{eu}(2)$ and the euphotic depths are deeper than the depth of integration Z_z for net community production (NCP), net primary production (NPP), and heterotrophic respiration (HR). Gray line represents the biomass-normalized HR. Red and green lines represent biomass-normalized NPP with $Z_{eu}(1)$ and $Z_{eu}(2)$, respectively. $Z_{eu}(1) > Z_{eu}(2)$ implies that light attenuation for the red line is weaker than for the green line. The export ratios for $Z_{eu}(1)$ and $Z_{eu}(2)$ are $ef_z(1) = \frac{b+c}{a+b+c}$ and $ef_z(2) = \frac{b}{a+b}$, where a, b, and c represent the areas of the hatched regions. Geometrically, $ef_z(1) = \frac{b+c}{a+b+c} > ef_z(2) = \frac{b}{a+b}$.

$$\begin{aligned} \mathrm{NCP}(0,Z_z) &= \mathrm{NPP}(0,Z_z) - \mathrm{HR}(0,Z_z) = \int_0^{Z_z}\mathrm{NPP}(z)\mathrm{d}z - \int_0^{Z_z}\mathrm{HR}(z)\mathrm{d}z \\ &= N_m \times I_m(0,Z_z) \times \mu_{\max} \times C - r_{\mathrm{HR}} \times C \times Z_z \end{aligned} \tag{15}$$

$$ef_z = \frac{\mathrm{NCP}(0,Z_z)}{\mathrm{NPP}(0,Z_z)} = 1 - \frac{1}{\overline{I_z}} \times \frac{1}{N_m} \times \frac{r_{\mathrm{HR}}}{\mu_{\max}} \tag{16a}$$

$$ef_z = \frac{\mathrm{NCP}(0,Z_z)}{\mathrm{NPP}(0,Z_z)} = 1 - \frac{\overline{I_{\mathrm{eu}}}}{\overline{I_z}}(1 - ef_{\mathrm{eu}}) \tag{16b}$$

where $\overline{I_z} = \frac{I_m(0,Z_z)}{Z_z}$ represents the averaged effect of light availability on the phytoplankton growth rate above a fixed depth Z_z. $\overline{I_z}$ decreases with increasing [Chl]. $I_m(0,Z_z) = \int_0^{Z_z} I_m(z)\mathrm{d}z = -\frac{1}{K_l} \times \ln\left(\frac{I_0 \times e^{-K_l \times Z_z} + k_m^I}{I_0 + k_m^I}\right)$ denotes the integrated effect of light availability on phytoplankton growth rate above the depth Z_z. The term $\overline{I_z}$ in equations (16a) and (16b) is a function of the optical depth of Z_z (i.e., $Z_z \times K_l$). The ef_z decreases with increasing Z_z, [Chl], and optical depth ($Z_z \times K_l$) as schematically shown in Figure 2b. As equations (16a) and (16b) can be rewritten as $ef_z = \frac{\mathrm{NCP}(0,Z_z)}{\mathrm{NPP}(0,Z_z)} = 1 - \frac{\mathrm{HR}(0,Z_z)}{\mathrm{NPP}(0,Z_z)} = 1 - \frac{\frac{\mathrm{HR}(0,Z_z)}{C}}{\frac{\mathrm{NPP}(0,Z_z)}{C}}$, these results can be alternatively explained by the biomass-normalized NPP ($\frac{\mathrm{NPP}(0,Z_z)}{C}$) (i.e., the autotrophic growth rate) decreasing with increasing [Chl] due to light attenuation, while the biomass-normalized HR ($\frac{\mathrm{HR}(0,Z_z)}{C}$) is insensitive to changes in [Chl].

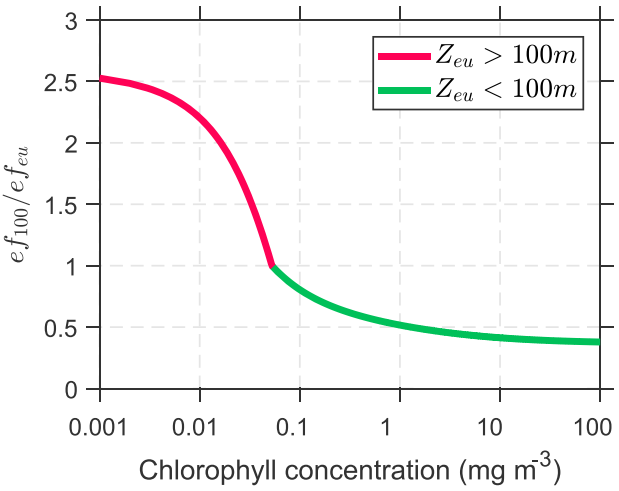

Figure 3. Export ratio at 100 m (ef_{100}) normalized to the export ratio at the euphotic depth (ef_{eu}) as a function of the chlorophyll *a* concentration. The ef_{100} is calculated from equations (14), (16a), and (16b). The ef_{eu} is derived using equation (9). We select a remineralization length scale of $Z^* = 100$ m, a half-saturation constant for photosynthetically active radiation of $k_m^I = 4.1$ E·m^{-2}·day^{-1}, and a surface radiation beneath the water surface of $I_0 = 50$ E·m^{-2}·day^{-1}. To calculate ef_{100}/ef_{eu} when the euphotic depth is deeper than 100 m, we set $ef_{eu} = 0.2$ which is in line with the typical value for the global ocean. Note that the abscissa is on a logarithmic scale.

3.3. Comparison to Other Export Ratio Algorithms

Rearranging and taking the natural logarithm of equation (9) yields

$$\ln(1 - ef_{eu}) = (B_t - P_t)\times T + \ln(\beta) + \ln\left(\frac{1}{\overline{I_{eu}}}\right) + \ln\left(\frac{1}{N_m}\right) \quad (17)$$

In sum, the controls on the export efficiency can be decomposed into four components: (1) the temperature dependence of the balance between autotrophic and heterotrophic processes ($(B_t - P_t) \times T$), (2) the community structure ($\ln(\beta)$), (3) the effect of light availability on the phytoplankton growth rate, and (4) the effect of nutrient availability on the phytoplankton growth rate. Missing or misrepresenting one of these components may impair the accuracy of satellite export production estimates. Equation (17) may be further simplified to

$$ef_{eu} = -(B_t - P_t)\times T - \ln(\beta) + \ln\left(\overline{I_{eu}}\right) + \ln(N_m) \quad (18)$$

based on the rough first-order approximation ($\ln(1 - ef_{eu}) \approx -ef_{eu}$ with increasing errors as $ef_{eu} \to 1$). If $(B_t - P_t)$ in equation (18) is a constant, ef_{eu} is a negative linear function of temperature, consistent in form with the empirical model of Dunne et al. (2005): $pe_r = -0.0081\times T + 0.0668\times \ln\left(\frac{Chl}{Z_{eu}}\right) + 0.426$, where pe_r is the particulate export ratio and Chl in this case reflects the chlorophyll inventory over the euphotic zone. Alternatively, if the temperature dependence $(B_t - P_t)$ relates to NPP, equation (18) is more in line with the empirical equations in Laws et al. (2011): $ef = -\frac{0.0165\times tp}{51.7+tp}\times T + \frac{0.5857\times tp}{51.7+tp}$ and $ef = -\frac{0.43\times tp^{0.307}}{30}\times T + 0.04756\times 0.78\times tp^{0.307}$, where tp is defined as NPP in Laws et al. (2011). The term $-\ln(\beta)$ in equation (18) may correspond to the $\ln\left(\frac{Chl}{Z_{eu}}\right)$ term in Dunne et al. (2005) because β is associated with phytoplankton community structure, which is in turn correlated with [Chl] (Agawin et al., 2000; Brewin et al., 2010; Sathyendranath et al., 2001). The term $\ln\left(\overline{I_{eu}}\right)$ varies as a function of I_0 but also depends on [Chl] when integration is to a fixed depth (equations (14), (16a), and (16b)). The terms $\ln\left(\overline{I_{eu}}\right)$ and $\ln(N_m)$ are not directly taken into account by some earlier models but are indirectly taken into account through NPP and [Chl] as in Dunne et al. (2005) and Laws et al. (2011).

3.4. Comparison of the Export Ratio at the Base of the Euphotic Layer and at 100 m

As an example of the effect of the depth of integration, we derive a functional relationship between ef_z at 100 m (ef_{100}) and at the euphotic depth (ef_{eu}) using equations ((9), (14), (16a), and (16b)), noting that our conclusions are valid for any other depths of integration. We select a remineralization length scale of $Z^* = 100$ m, a half-saturation constant for radiation of $k_m^I = 4.1$ E·m^{-2}·day^{-1}, and the monthly climatology of ef_{100} estimated using the algorithm of Dunne et al. (2005). Monthly climatology of SST, chlorophyll *a* concentration, and PAR was downloaded from the ocean color website (https://oceancolor.gsfc.nasa.gov/). We use these data products to calculate the euphotic depth and ef_{100}/ef_{eu} based on equations (7) and (8).

When Z_{eu} is deeper than 100 m ($Z_{eu} > 100$), $\frac{1 - ef_{100}}{1 - ef_{eu}} = \frac{\overline{I_{eu}}}{\overline{I_{100}}} < 1$ can be obtained by reorganizing equations (9), (16a), and (16b), where $\overline{I_{100}}$ is the averaged effect of light availability on the phytoplankton growth rate above 100 m. This relationship suggests that $\frac{ef_{100}}{ef_{eu}}$ is greater than 1 ($\frac{ef_{100}}{ef_{eu}} > 1$) and rapidly decreases with increasing [Chl] (due to decreasing $\overline{I_{100}}$ but no change in $\overline{I_{eu}}$), as shown in the schematic diagram in Figure 3. In the subtropical gyres, where Z_{eu} is often deeper than 100 m due to extremely low [Chl] (e.g., [Chl] = 0.01 mg/m^3 leads to $Z_{eu} = 192.66$ m), ef_{100} could be as much as 7 times larger than ef_{eu} (Figure 4).

When Z_{eu} is shallower than 100 m ($Z_{eu} < 100$), a simple reorganization of equation (14) yields $\frac{ef_{100}}{ef_{eu}} = e^{-\frac{100 - Z_{eu}}{Z^*}}$. This equation suggests that $\frac{ef_{100}}{ef_{eu}}$ is smaller than 1 ($\frac{ef_{100}}{ef_{eu}} < 1$), and that an increase in [Chl] again decreases Z_{eu}

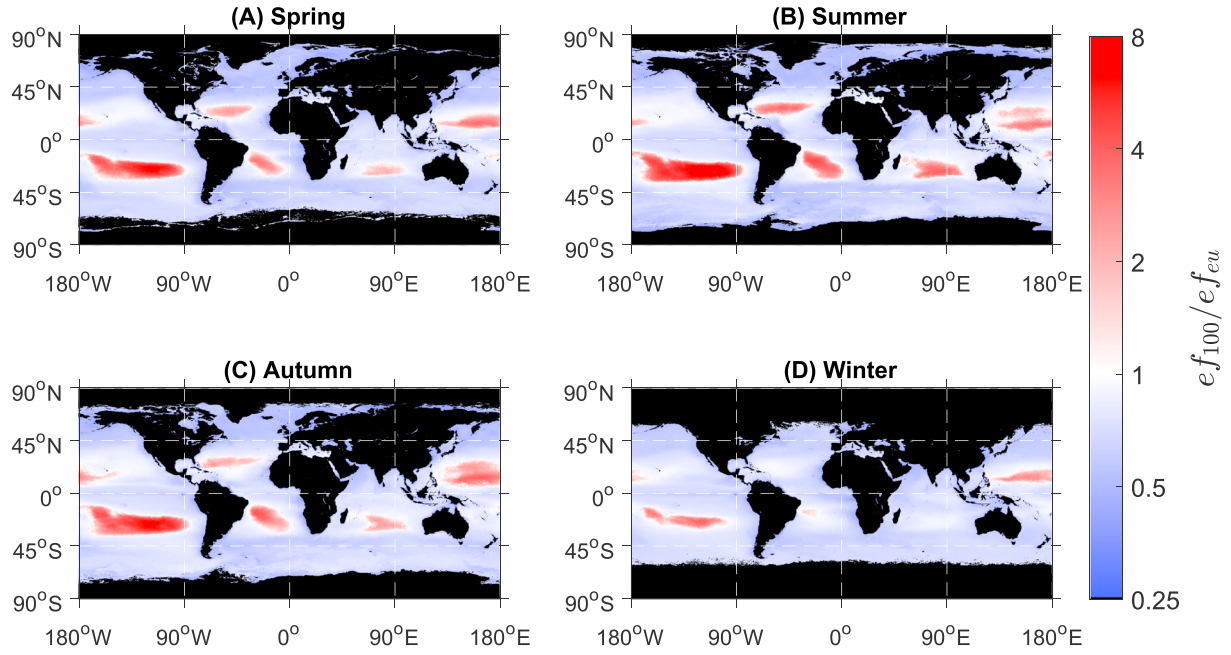

Figure 4. Global distribution of seasonally averaged ef_{100}/ef_{eu}. The ef_{100} is calculated from equations (14), (16a), and (16b). The ef_{eu} is derived using equation (9). In the Northern Hemisphere, seasons are defined as follows: (a) spring (March–May), (b) summer (June–August), (c) autumn (September–November), and (d) winter (December–February). In the Southern Hemisphere, seasons are defined as follows: spring (September–November), summer (December–February), autumn (March–May), and winter (June–August). Note that the ratio is shown on a logarithmic scale.

and hence $\frac{ef_{100}}{ef_{eu}}$ (Figure 3). However, $\frac{ef_{100}}{ef_{eu}}$ is less sensitive to changes in [Chl] than when $Z_{eu} > 100$ (Figure 3). For example, ef_{100} is less than half of ef_{eu} in regions with very high [Chl] (e.g., Southern Ocean and coastal regions; [Chl] = 10 mg/m^3 gives Z_{eu} = 11.66 m and $\frac{ef_{100}}{ef_{eu}} = 0.41$ for Z^* = 100 m).

These considerations may in part explain the large discrepancies between satellite algorithms in predictions of export production in the subtropical regions, the Southern Ocean, and the Arctic Ocean (Li & Cassar, 2016). In these regions, extremely low and high [Chl] regimes are observed. Some algorithms predict the *ef* ratio at the euphotic depth (Eppley & Peterson, 1979; Laws et al., 2000; Siegel et al., 2014) while others at a given depth such as the MLD (Li & Cassar, 2016) or 100 m (Dunne et al., 2005; Henson et al., 2011; Le Moigne et al., 2016; Maiti et al., 2013). Differing integration depths could also explain the reported inconsistent relationship between *ef* ratio and gross primary product (Hendricks et al., 2004) and NPP (Maiti et al., 2013).

The *ef* ratios measured at different depths display similar functionalities (equations (9), (14), (16a), and (16b)); however, integrating to the euphotic depths may be preferable. First, as opposed to the euphotic depth, which has a clear influence on phytoplankton physiology, a physical depth's influence on the *ef* ratio changes with light attenuation, preventing the exploration of controls (e.g., plankton community structure) on the *ef* ratio across regions with different [Chl]. An *ef* ratio measured shallower than the euphotic depth misses parts of the particles produced. Conversely, an *ef* ratio measured deeper than the euphotic depth disproportionately reflects particle destruction processes.

There are practical reasons to measure the *ef* ratio at depth. For example, shallow sediment traps are notoriously unreliable (Buesseler, 1991). However, as shown in equation (14), export at depth can be modeled as a function of ef_{eu} and flux attenuation below the euphotic depth, albeit with significant uncertainties. Because controls on the ef_{eu} and the transfer efficiency are likely different (Buesseler & Boyd, 2009; Lima et al., 2014), this two-step approach likely improves predictions of the strength of the biological pump. Our results also underscore Buesseler and Boyd (2009) recommendation to account for variations in Z_{eu} when reporting export or *ef* ratios.

4. Influence of Environmental Properties on the Export Ratio

In order to gain some quantitative intuition into how N, I_0, T, [Chl], and MLD influence the ef ratio, we take the partial derivative of ef_z at the base of the mixed layer (ef_{ml}) relative to each property in equations (16a) and (16b):

$$\frac{\partial ef_{\mathrm{ml}}}{\partial N} = N_m \times \frac{k_m^N}{N^2} \times (1 - ef_{\mathrm{ml}}) \tag{19}$$

$$\frac{\partial ef_{\mathrm{ml}}}{\partial I_0} = \frac{I_m(\mathrm{MLD}) \times \left(e^{K_I \times \mathrm{MLD}} - 1\right)}{I_m(0, \mathrm{MLD}) \times K_I} \times \frac{k_m^I}{\left(I_0 + k_m^I\right) \times \mathrm{I_0}} \times (1 - ef_{\mathrm{ml}}) \tag{20}$$

$$\frac{\partial ef_{\mathrm{ml}}}{\partial T} = -(B_t - P_t) \times (1 - ef_{\mathrm{ml}}) \tag{21}$$

$$\frac{\partial ef_{\mathrm{ml}}}{\partial [\mathrm{Chl}]} = -\left(1 - \frac{I_m(\mathrm{MLD})}{\overline{I_{\mathrm{ml}}}}\right) \times \frac{1}{K_I} \times \frac{\mathrm{d}K_I}{\mathrm{d}[\mathrm{Chl}]} \times (1 - ef_{\mathrm{ml}}) \tag{22}$$

$$\frac{\partial ef_{\mathrm{ml}}}{\partial \mathrm{MLD}} = -\left(1 - \frac{I_m(\mathrm{MLD})}{\overline{I_{\mathrm{ml}}}}\right) \times \frac{1}{\mathrm{MLD}} \times (1 - ef_{\mathrm{ml}}) \tag{23}$$

where $I_m(\mathrm{MLD}) = \frac{I_0 \times e^{-K_I \times \mathrm{MLD}}}{I_0 \times e^{-K_I \times \mathrm{MLD}} + k_m^I}$ represents the influence of light availability on phytoplankton growth rate at MLD; $\overline{I_{\mathrm{ml}}} = \frac{I_m(0, \mathrm{MLD})}{\mathrm{MLD}}$ represents the averaged effect of light availability on the phytoplankton growth rate within the mixed layer; $I_m(0, \mathrm{MLD})$ is the integrated effect of light availability on the phytoplankton growth rate over the mixed layer; and $\frac{\mathrm{d}K_I}{\mathrm{d}[\mathrm{Chl}]}$ can be derived from equations (5a) and (5b) and is positive ($\frac{\mathrm{d}K_I}{\mathrm{d}[\mathrm{Chl}]} > 0$). The derivations of equations (19)–(23) are presented in the supporting information. The ef_{ml} increases with N ($\frac{\partial ef_{\mathrm{ml}}}{\partial N} > 0$) and I_0 ($\frac{\partial ef_{\mathrm{ml}}}{\partial I_0} > 0$) due to increasing phytoplankton growth rate. The ef_{ml} decreases with T ($\frac{\partial ef_{\mathrm{ml}}}{\partial T} < 0$) because of the higher-temperature sensitivity of heterotrophic respiration compared to phytoplankton growth rate ($B_t > P_t$), in line with multiple previous studies (Cael & Follows, 2016; Dunne et al., 2005; Henson et al., 2011; Laws et al., 2011, 2000). The ef_{ml} decreases with [Chl] ($\frac{\partial ef_{\mathrm{ml}}}{\partial [\mathrm{Chl}]} < 0$) and MLD ($\frac{\partial ef_{\mathrm{ml}}}{\partial \mathrm{MLD}} < 0$) due to decreasing average light availability. In reality, a deepening of the mixed layer may also entrain nutrients from the subsurface, leading to an increase in ef_{ml} (equation (19)). This effect is not directly taken into account in our model. The balance of the effects of MLD deepening on nutrient and light availability ultimately determines how ef_{ml} varies with MLD. Equations (19)–(23) can be applied to ef_{eu}, with the exception that ef_{eu} is independent of [Chl] and the depth of integration ($\frac{\partial ef_{\mathrm{eu}}}{\partial [\mathrm{Chl}]} = \frac{\partial ef_{\mathrm{eu}}}{\partial Z_{\mathrm{eu}}} = 0$). In some studies, ef_z is derived from taking the ratio of export (or NCP) measurements integrated to a certain depth (e.g., 100 m or MLD) to NPP integrated over the euphotic depth. Under such circumstances, the sign of $\frac{\partial ef_z}{\partial [\mathrm{Chl}]}$ varies, with ef ratio displaying a bell-shaped relation to [Chl] (see Figure S1 in the supporting information).

4.1. Relation Between the Export Ratio at a Fixed Depth and NPP

Recent studies have reported a negative relation between NPP and ef_{100} in the Southern Ocean (Le Moigne et al., 2016; Maiti et al., 2013), in contrast to earlier studies (Dunne et al., 2005; Eppley & Peterson, 1979; Laws et al., 2011, 2000). Relating the ef ratio to NPP could lead to spurious negative correlations of the type x versus (a/x) where a is a constant. This is especially the case for deep depths of integration because geographical variability in export production decreases with increasing depth (Antia et al., 2001; Henson et al., 2012). While we cannot rule out that the negative correlation between the ef ratio and NPP results from a mathematical tautology, others have hypothesized that it results from grazing and fecal-mediated export (Cavan et al., 2017; Le Moigne et al., 2016), temperature (Henson et al., 2015), and DOC export (Hansell et al., 2009; Maiti et al., 2013). Many of these factors are encapsulated in the β term relating r_{HR} to μ_{max} in equation (12). The β reflects community structure that is in turn related [Chl] and NPP (Lopez-Urrutia et al., 2006). While the cause remains unknown, our models provide an additional explanation for the reported discrepancies in the relationship between ef_{100} and NPP. NPP is the product of phytoplankton biomass (C) and growth rate (μ). All other factors equal, euphotic depth integrated NPP is a positive function of C (Figure 1). Since ef_{100}

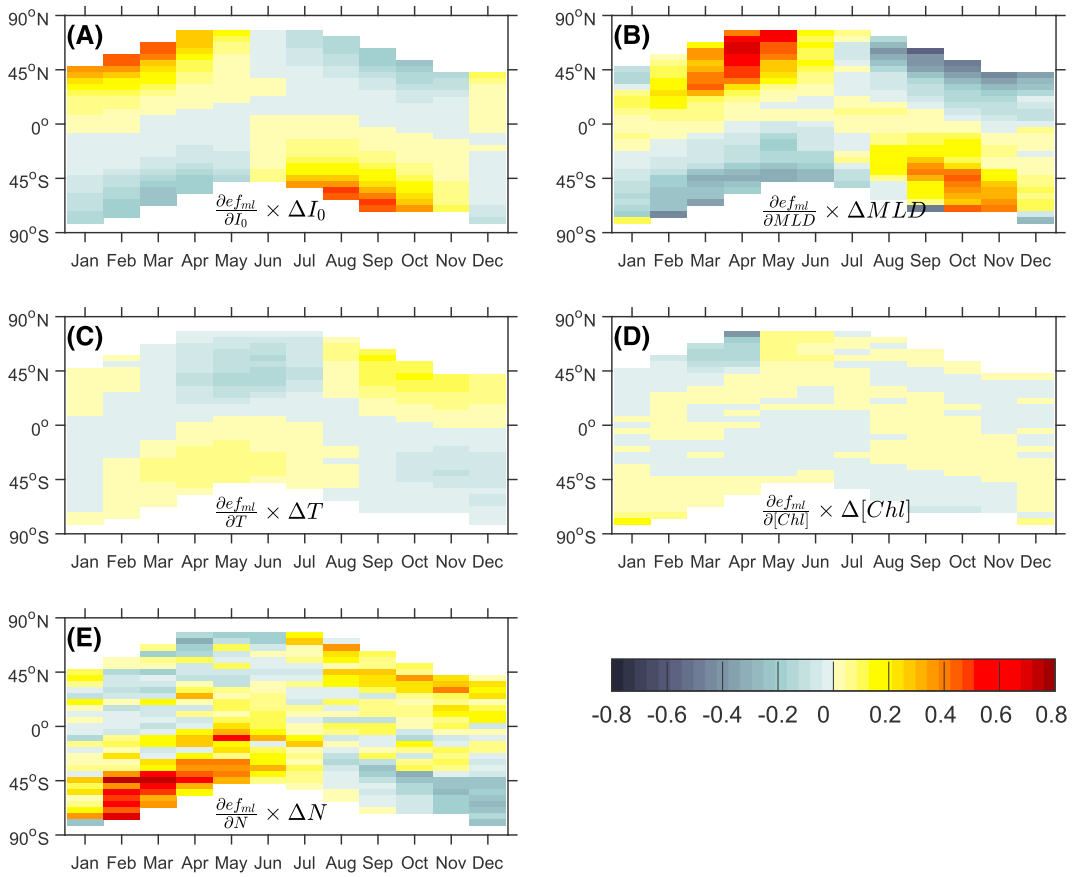

Figure 5. Hofmøller plots of the climatology of seasonal variations in the export ratio at the base of the mixed layer due to (a) photosynthetically active radiation just beneath water surface (I_0), (b) mixed layer depth (MLD), (c) sea surface temperature (T), (d) chlorophyll *a* concentration ([Chl]), and (e) nutrient concentration (N). Horizontal and vertical axes represent months and latitudes, respectively. Each row reflects a zonal average for each month. White areas represent missing values. Calculations are based on equation (24), noting that since $1 - ef_{ml}$ is included in equations (19)–(23) describing all individual parameters, it is normalized in the derivation. See the supporting information for the spatial distribution of each (a–e) contribution.

is a negative function of [Chl], an increase in NPP due to high C will decrease ef_{100} (Figure 2). Conversely, if the increase in NPP stems from other factors such as increasing nutrient and light availability (i.e., higher autotrophic growth rate), ef_{100} is expected to positively correlate with NPP.

4.2. Seasonal Variability in the Export Ratio at the Base of the Mixed Layer

Based on equations (19)–(23), we decompose the seasonal controls on ef_{ml} as the sum of partial differentials:

$$\Delta ef_{ml} = \frac{\partial ef_{ml}}{\partial N} \times \Delta N + \frac{\partial ef_{ml}}{\partial I_0} \times \Delta I_0 + \frac{\partial ef_{ml}}{\partial T} \times \Delta T + \frac{\partial ef_{ml}}{\partial [Chl]} \times \Delta [Chl] + \frac{\partial ef_{ml}}{\partial MLD} \times \Delta MLD \quad (24)$$

where Δef_{ml} denotes the total differential of ef_{ml}; and ΔN, ΔI_0, ΔT, Δ[Chl], and ΔMLD represent changes in N, I_0, T, [Chl], and MLD, respectively. As $1 - ef_{ml}$ appears in all the individual equations (19)–(23), it is not required to estimate the relative contribution of each term in equation (24). We estimate I_0, T, and [Chl] from satellite data, MLD from the climatology of de Boyer Montegut et al. (2004), and N from World Ocean Atlas monthly climatologies (Garcia et al., 2014). Details on data and the derivation of seasonal changes in nutrient availability are presented in the supporting information (Boyd et al., 2000; Boyd & Ellwood, 2010; Cassar et al., 2007; Deutsch et al., 2007; Johnson et al., 1997; Martin et al., 1990; Mitchell et al., 1991; Mitchell & Holm-Hansen, 1991; Moore et al., 2013; Nelson & Smith, 1991; Sarmiento & Gruber, 2006). Figure 5 shows how seasonal variations in ef_{ml} are impacted by I_0, MLD, T, [Chl], and N. Among these factors, I_0 and MLD dominate seasonal variability in ef_{ml} at high latitude. In the spring, ef_{ml} sharply increases with increasing I_0 and shoaling MLD ($\frac{\partial ef_{ml}}{\partial I_0}$

$\times\Delta I_0 > 0$ and $\frac{\partial ef_{ml}}{\partial MLD}\times\Delta\text{MLD} > 0$). In contrast, decreasing I_0 and deepening MLD in the autumn lead to a decrease in ef_{ml} ($\frac{\partial ef_{ml}}{\partial I_0}\times\Delta I_0 < 0$ and $\frac{\partial ef_{ml}}{\partial \text{MLD}}\times\Delta\text{MLD} < 0$). Our results are consistent with the dominant controls of MLD and I_0 on NCP in the Southern Ocean on seasonal time scales (Li, 2017).

T also contributes to the seasonal variability in ef_{ml}. Interestingly, $\frac{\partial ef_{ml}}{\partial T}\times\Delta T$ is higher in polar regions. Similarly, [Chl] affects the seasonality in ef_{ml} north 45°N in March and April. However, $\frac{\partial ef_{ml}}{\partial [\text{Chl}]}\times\Delta[\text{Chl}]$ shows large spatial variability (see the supporting information). Conversely, N mostly impacts the seasonality of ef_{ml} in the Southern Ocean. The $\frac{\partial ef_{ml}}{\partial N}\times\Delta N$ leads to an increase in ef_{ml} in late austral summer early autumn due to deepening mixed layers, in part counteracting the decreasing light availability associated with I_0 and deepening mixed layers. Additionally, our data support equation (19)'s prediction that ef_{ml} is particularly sensitive to variations in nutrient availability when nutrient concentrations are low (see the supporting information). Because of the assumptions going into the derivation of N, it is likely the parameter with the most uncertain effect on ef_{ml}. Uncertainties, assumptions, and simplifications associated with $\frac{\partial ef_{ml}}{\partial N}\times\Delta N$ are discussed in the section on caveats and limitations. Overall, our results emphasize that caution should be exercised when interpreting ef_{ml} across regions and seasons because of varying I_0, MLD, T, [Chl], and N.

5. Caveats, Limitations, Additional Considerations, and Future Improvements

Below we enumerate some of the assumptions and simplifications that go into the construction of our model. While they introduce uncertainties, they do not change our main conclusions that fundamental factors confound the interpretation of the *ef* ratio.

Photophysiology: Modeling the influence of light availability on phytoplankton growth assuming Michaelis-Menten kinetics does not account for light inhibition and photoacclimation (Geider, 1987; Geider et al., 1996, 1998; Jassby & Platt, 1976; Pahlow & Oschlies, 2009). In addition, K_I varies with depth due to the optional attenuation of PAR (see Li & Cassar, 2017, and references therein), with the relationship between K_I and [Chl] also being impacted by other factors, including detritus, colored dissolved organic matter, and solar zenith angle (Gordon, 1989). We also note that defining the euphotic depth based on a percentage of surface irradiance has been shown to be of little physiological significance (Banse, 2004; Laws et al., 2014; Letelier et al., 2004; Lorenzen, 1976; Marra et al., 2014). While our model can readily be adapted to reflect a depth more meaningful to photochemistry, for the purpose of this study, the definition in equation (8) is adequate.

Stoichoimetry: The elemental stoichiometry and half-saturation constants of marine phytoplankton are known to vary with seasonal changes in growth conditions and species (Eppley et al., 1969; Moreno & Martiny, 2018; Smith et al., 2009). Our model does not account for this variability and assumes that the concentrations and half-saturation constants of limiting and nonlimiting factors vary proportionally. All these simplifications and top-down controls on the phytoplankton growth rate (as opposed to nutrients) will need to be further evaluated.

Other biogeochemical and trophic processes: By design, our metabolism-based model prescinds complex biogeochemical processes represented in food web models. While our modeling of autotrophy is on par with more complex food web models (e.g., Nutrient-Phytoplankton-Zooplankton-Detritus), our representation of heterotrophy being a simple function of temperature and biomass does not reflect the panoply of biogeochemical and trophic processes influencing organic carbon loss from the system. For example, our model does not represent the process of particle aggregation, which is believed to be a first-order control on the *ef* ratio (Boyd & Trull, 2007; Burd & Jackson, 2009; Passow et al., 1994). Aggregation with rapid sinking would lead to lower surface respiration and higher *ef* ratios than predicted based on the model's temperature parameterization. The temperature dependence of r_{HR} and μ_{max} have large uncertainties (see Li & Cassar, 2017, and references therein). Variations in the relative proportion of POC and DOC production associated with NCP, attributed to food web processes and plankton's physiological status (Emerson, 2014; Hansell & Carlson, 1998; Hygum et al., 1997; Thornton, 2014), are also not included in our modeling effort.

Our model assumes steady state. A lack of steady state may lead to two types of biases, natural and methodological. First, export efficiency observations may be biased when export lags production (Buesseler, 1998; Buesseler et al., 2009; Henson et al., 2015), in which case the *ef* ratio would be underestimated (overestimated) in the production (export) phase. This is particularly important in physically dynamic and

biologically sluggish (low-temperature) systems such as the Southern Ocean. Second, differences in integration time scales of export production and NPP bias estimates of the *ef* ratio in systems that are not at steady state. For example, export production measurements (~24 days based on ^{234}Th) usually have longer integration time scales than NPP estimates (~1 day).

Vertical profiles: For simplicity, we assume that μ_{max}, r_{HR}, N, k_m^N, k_m^I, [Chl], and C are well mixed or constant within the euphotic zone and mixed layer. However, these parameters may vary within the mixed layer, especially for water columns with limited turbulent mixing. In the subtropical regions where the water column is well stratified, low nutrient availability often leads to euphotic zones that are deeper than the mixed layer, and as a result some parameters (e.g., N, [Chl], and C) beneath the mixed layer may differ from those within the mixed layer.

6. Conclusions

In this study, we developed a metabolism-based mechanistic model to explore how fundamental factors may confound the interpretation of field observations of the export ratio (*ef* ratio). Our results show that the effect of trophic processes and community composition on the export efficiency may be masked by changes in temperature, biomass, and light availability. As such, analyses of the impact of biological and biogeochemical processes on ef_{ml} should be interpreted with caution, especially in high latitudes where variations in ef_{ml} are dominated by MLD and surface radiation over seasonal time scales. Our approach also offers a new framework for relating phytoplankton size composition to field estimates, satellite algorithms, and Earth system models of the *ef* ratio. Finally, our theoretical considerations provide further support for reporting or normalizing field observations of the *ef* ratio to the euphotic depth. While the best depth horizon for reporting *ef* ratio may depend on the process under study, our modeling effort shows that estimating *ef* ratios at a depth other than the euphotic depth (e.g., 100 m or MLD) complicates the interpretation of the temporal and spatial variability in the *ef* ratio.

More fundamentally, our study demonstrates that it may be time to revisit the export ratio proxy. In their classical paper, Eppley and Peterson (1979) first recommended normalizing new production to primary production (*f* ratio) as the "total flux seems to be approximately proportional to the plankton production in the overlying water." While normalization by ratio correction is commonly applied in life sciences to account for the effect of a confounding variable, it is known to be flawed (Karp et al., 2012, and references therein). In addition to the issues associated with ratio corrections, our theoretical considerations above demonstrate that export is not a simple function of NPP. Identical NPP resulting from differing autotrophic biomass and growth rates may lead to differing export ratios. These mathematical and biogeochemical shortcomings with the export ratio thus argue for the development of more ecumenical proxies of the biological pump.

Acknowledgments
Z. L was supported by a NASA Earth and Space Science Fellowship (Grant NNX13AN85H) and the Postdoctoral Scholarship Program at Woods Hole Oceanographic Institution. N. C. was supported by NASA Grant 5109296. Satellite data, nutrient concentration, and monthly MLD climatology are downloaded from NASA ocean color (http://oceancolor.gsfc.nasa.gov/cms/), World Ocean Atlas (https://www.nodc.noaa.gov/OC5/woa13/), and http://www.ifremer.fr/cerweb/deboyer/mld/home.php, respectively.

References

Agawin, N. S. R., Duarte, C. M., & Agusti, S. (2000). Nutrient and temperature control of the contribution of picoplankton to phytoplankton biomass and production. *Limnology and Oceanography*, *45*(3), 591–600. https://doi.org/10.4319/lo.2000.45.3.0591

Aksnes, D. L., & Wassmann, P. (1993). Modeling the significance of zooplankton grazing for export production. *Limnology and Oceanography*, *38*(5), 978–985. https://doi.org/10.4319/lo.1993.38.5.0978

Alldredge, A. L., & Silver, M. W. (1988). Characteristics, dynamics and significance of marine snow. *Progress in Oceanography*, *20*(1), 41–82. https://doi.org/10.1016/0079-6611(88)90053-5

Antia, A. N., Koeve, W., Fischer, G., Blanz, T., Schulz-Bull, D., Schölten, J., Neuer, S., et al. (2001). Basin-wide particulate carbon flux in the Atlantic Ocean: Regional export patterns and potential for atmospheric CO_2 sequestration. *Global Biogeochemical Cycles*, *15*(4), 845–862. https://doi.org/10.1029/2000GB001376

Armstrong, R. A., Lee, C., Hedges, J. I., Honjo, S., & Wakeham, S. G. (2002). A new, mechanistic model for organic carbon fluxes in the ocean based on the quantitative association of POC with ballast minerals. *Deep-Sea Res Pt Ii*, *49*(1–3), 219–236.

Arrigo, K. R., van Dijken, G. L., & Bushinsky, S. (2008). Primary production in the Southern Ocean, 1997–2006. *Journal of Geophysical Research*, *113*, C08004. https://doi.org/10.1029/2007JC004551

Baines, S. B., Pace, M. L., & Karl, D. M. (1994). Why does the relationship between sinking flux and planktonic primary production differ between lakes and oceans. *Limnology and Oceanography*, *39*(2), 213–226. https://doi.org/10.4319/lo.1994.39.2.0213

Banse, K. (2004). Should we continue to use the 1% light depth convention for estimating the compensation depth of phytoplankton for another 70 years? *Limnology and Oceanography Bulletin*, *13*(3), 49–52. https://doi.org/10.1002/lob.200413349

Behrenfeld, M. J., & Falkowski, P. G. (1997). Photosynthetic rates derived from satellite-based chlorophyll concentration. *Limnology and Oceanography*, *42*, 1–20.

Betzer, P. R., Showers, W. J., Laws, E. A., Winn, C. D., Ditullio, G. R., & Kroopnick, P. M. (1984). Primary productivity and particle fluxes on a transect of the equator at 153°W in the Pacific Ocean. *Deep Sea Research Part A*, *31*(1), 1–11.

Boyd, P., & Newton, P. (1995). Evidence of the potential influence of planktonic community structure on the interannual variability of particulate organic carbon flux. *Deep Sea Research Part I*, *42*(5), 619–639. https://doi.org/10.1016/0967-0637(95)00017-Z

Boyd, P. W., & Ellwood, M. J. (2010). The biogeochemical cycle of iron in the ocean. *Nature Geoscience*, *3*(10), 675–682. https://doi.org/10.1038/ngeo964

Boyd, P. W., & Newton, P. P. (1999). Does planktonic community structure determine downward particulate organic carbon flux in different oceanic provinces? *Deep-Sea Research Part I*, *46*(1), 63–91. https://doi.org/10.1016/S0967-0637(98)00066-1

Boyd, P. W., & Trull, T. W. (2007). Understanding the export of biogenic particles in oceanic waters: Is there consensus? *Progress in Oceanography*, *72*(4), 276–312. https://doi.org/10.1016/j.pocean.2006.10.007

Boyd, P. W., Watson, A. J., Law, C. S., Abraham, E. R., Trull, T., Murdoch, R., Bakker, D. C. E., et al. (2000). A mesoscale phytoplankton bloom in the polar Southern Ocean stimulated by iron fertilization. *Nature*, *407*(6805), 695–702. https://doi.org/10.1038/35037500

Brewin, R. J. W., Sathyendranath, S., Hirata, T., Lavender, S. J., Barciela, R., & Hardman-Mountford, N. J. (2010). A three-component model of phytoplankton size class for the Atlantic Ocean. *Ecological Modelling*, *221*(11), 1472–1483. https://doi.org/10.1016/j.ecolmodel.2010.02.014

Britten, G. L., Wakamatsu, L., & Primeau, F. W. (2017). The temperature-ballast hypothesis explains carbon export efficiency observations in the Southern Ocean. *Geophysical Research Letters*, *44*, 1831–1838. https://doi.org/10.1002/2016GL072378

Buesseler, K. O. (1991). Do upper-ocean sediment traps provide an accurate record of particle flux? *Nature*, *353*(6343), 420–423. https://doi.org/10.1038/353420a0

Buesseler, K. O. (1998). The decoupling of production and particulate export in the surface ocean. *Global Biogeochemical Cycles*, *12*(2), 297–310. https://doi.org/10.1029/97GB03366

Buesseler, K. O., & Boyd, P. W. (2009). Shedding light on processes that control particle export and flux attenuation in the twilight zone of the open ocean. *Limnology and Oceanography*, *54*(4), 1210–1232. https://doi.org/10.4319/lo.2009.54.4.1210

Buesseler, K. O., Pike, S., Maiti, K., Lamborg, C. H., Siegel, D. A., & Trull, T. W. (2009). Thorium-234 as a tracer of spatial, temporal and vertical variability in particle flux in the North Pacific. *Deep Sea Research, Part I*, *56*(7), 1143–1167. https://doi.org/10.1016/j.dsr.2009.04.001

Burd, A. B., & Jackson, G. A. (2009). Particle aggregation. *Annual Review of Marine Science*, *1*(1), 65–90. https://doi.org/10.1146/annurev.marine.010908.163904

Cael, B. B., & Follows, M. J. (2016). On the temperature dependence of oceanic export efficiency. *Geophysical Research Letters*, *43*, 5170–5175. https://doi.org/10.1002/2016GL068877

Cassar, N., Bender, M. L., Barnett, B. A., Fan, S., Moxim, W. J., Levy, H., & Tilbrook, B. (2007). The Southern Ocean biological response to aeolian iron deposition. *Science*, *317*(5841), 1067–1070. https://doi.org/10.1126/science.1144602

Cavan, E. L., Henson, S. A., Belcher, A., & Sanders, R. (2017). Role of zooplankton in determining the efficiency of the biological carbon pump. *Biogeosciences*, *14*(1), 177–186. https://doi.org/10.5194/bg-14-177-2017

Cavan, E. L., Le Moigne, F. A. C., Poulton, A. J., Tarling, G. A., Ward, P., Daniels, C. J., Fragoso, G. M., et al. (2015). Attenuation of particulate organic carbon flux in the Scotia Sea, Southern Ocean, is controlled by zooplankton fecal pellets. *Geophysical Research Letters*, *42*, 821–830. https://doi.org/10.1002/2014GL062744

de Boyer Montegut, C., Madec, G., Fischer, A. S., Lazar, A., & Iudicone, D. (2004). Mixed layer depth over the global ocean: An examination of profile data and a profile-based climatology. *Journal of Geophysical Research*, *109*, C12003. https://doi.org/10.1029/2004JC002378

Deutsch, C., Sarmiento, J. L., Sigman, D. M., Gruber, N., & Dunne, J. P. (2007). Spatial coupling of nitrogen inputs and losses in the ocean. *Nature*, *445*(7124), 163–167. https://doi.org/10.1038/nature05392

Dugdale, R. C., & Goering, J. J. (1967). Uptake of new and regenerated forms of nitrogen in primary productivity. *Limnology and Oceanography*, *12*(2), 196–206. https://doi.org/10.4319/lo.1967.12.2.0196

Dunne, J. P., Armstrong, R. A., Gnanadesikan, A., & Sarmiento, J. L. (2005). Empirical and mechanistic models for the particle export ratio. *Global Biogeochemical Cycles*, *19*, GB4027. https://doi.org/10.1029/2004GB002390

Dutkiewicz, S., Follows, M., Marshall, J., & Gregg, W. W. (2001). Interannual variability of phytoplankton abundances in the North Atlantic. *Fibiger*, *48*(10), 2323–2344. https://doi.org/10.1016/S0967-0645(00)00178-8

Emerson, S. (2014). Annual net community production and the biological carbon flux in the ocean. *Global Biogeochemical Cycles*, *28*, 14–28. https://doi.org/10.1002/2013GB004680

Eppley, R. W. (1972). Temperature and phytoplankton growth in the sea. *Fishery Bulletin*, *70*(4), 1063–1085.

Eppley, R. W., & Peterson, B. J. (1979). Particulate organic matter flux and planktonic new production in the deep ocean. *Nature*, *282*(5740), 677–680. https://doi.org/10.1038/282677a0

Eppley, R. W., Rogers, J. N., & Mccarthy, J. J. (1969). Half-saturation constants for uptake of nitrate and ammonium by marine phytoplankton. *Limnology and Oceanography*, *14*(6), 912–920. https://doi.org/10.4319/lo.1969.14.6.0912

Francois, R., Honjo, S., Krishfield, R., & Manganini, S. (2002). Factors controlling the flux of organic carbon to the bathypelagic zone of the ocean. *Global Biogeochemical Cycles*, *16*(4), 1087. https://doi.org/10.1029/2001GB001722

Garcia, H. E., Locarnini, R. A., Boyer, T. P., Antonov, J. I., Baranova, O. K., Zweng, M. M., Reagan, J. R., et al. (2014). World Ocean Atlas 2013. In S. Levitus & A. Mishonov Technical (Eds.), *Dissolved inorganic nutrients (phosphate, nitrate, silicate)* (Vol. 4, p. 25). NOAA Atlas NESDIS 76.

Geider, R. J. (1987). Light and temperature-dependence of the carbon to chlorophyll-a ratio in microalgae and cyanobacteria: Implications for physiology and growth of phytoplankton. *The New Phytologist*, *106*(1), 1–34. https://doi.org/10.1111/j.1469-8137.1987.tb04788.x

Geider, R. J., MacIntyre, H. L., & Kana, T. M. (1996). A dynamic model of photoadaptation in phytoplankton. *Limnology and Oceanography*, *41*(1), 1–15. https://doi.org/10.4319/lo.1996.41.1.0001

Geider, R. J., MacIntyre, H. L., & Kana, T. M. (1998). A dynamic regulatory model of phytoplanktonic acclimation to light, nutrients, and temperature. *Limnology and Oceanography*, *43*(4), 679–694. https://doi.org/10.4319/lo.1998.43.4.0679

Gordon, H. R. (1989). Can the Lambert-Beer law be applied to the diffuse attenuation coefficient of ocean water? *Limnology and Oceanography*, *34*(8), 1389–1409. https://doi.org/10.4319/lo.1989.34.8.1389

Guidi, L., Chaffron, S., Bittner, L., Eveillard, D., Larhlimi, A., Roux, S., Darzi, Y., et al. (2016). Plankton networks driving carbon export in the oligotrophic ocean. *Nature*, *532*(7600), 465–470. https://doi.org/10.1038/nature16942

Hansell, D. A., & Carlson, C. A. (1998). Net community production of dissolved organic carbon. *Global Biogeochemical Cycles*, *12*(3), 443–453. https://doi.org/10.1029/98GB01928

Hansell, D. A., Carlson, C. A., Repeta, D. J., & Schlitzer, R. (2009). Dissolved organic matter in the ocean a controversy stimulates new insights. *Oceanography*, *22*(4), 202–211. https://doi.org/10.5670/oceanog.2009.109

Hendricks, M. B., Bender, M. L., & Barnett, B. A. (2004). Net and gross O_2 production in the Southern Ocean from measurements of biological O_2 saturation and its triple isotope composition. *Deep Sea Research Part I: Oceanographic Research Papers*, *51*(11), 1541–1561. https://doi.org/10.1016/j.dsr.2004.06.006

Henson, S. A., Sanders, R., & Madsen, E. (2012). Global patterns inefficiency of particulate organic carbon export and transfer to the deep ocean. *Global Biogeochemical Cycles*, *26*, GB1028. https://doi.org/10.1029/2011GB004099

Henson, S. A., Sanders, R., Madsen, E., Morris, P. J., Le Moigne, F., & Quartly, G. D. (2011). A reduced estimate of the strength of the ocean's biological carbon pump. *Geophysical Research Letters*, *38*, L04606. https://doi.org/10.1029/2011GL046735

Henson, S. A., Yool, A., & Sanders, R. (2015). Variability in efficiency of particulate organic carbon export: A model study. *Global Biogeochemical Cycles*, *29*, 33–45. https://doi.org/10.1002/2014GB004965

Huang, K., Ducklow, H., Vernet, M., Cassar, N., & Bender, M. L. (2012). Export production and its regulating factors in the West Antarctica Peninsula region of the Southern Ocean. *Global Biogeochemical Cycles*, *26*, GB2005. https://doi.org/10.1029/2010GB004028

Huisman, J., & Weissing, F. J. (1994). Light-limited growth and competition for light in well-mixed aquatic environments: An elementary model. *Ecology*, *75*(2), 507–520. https://doi.org/10.2307/1939554

Hygum, B. H., Petersen, J. W., & Søndergaard, M. (1997). Dissolved organic carbon released by zooplankton grazing activity—A high quality substrate pool for bacteria. *Journal of Plankton Research*, *19*(1), 97–111. https://doi.org/10.1093/plankt/19.1.97

Jackson, G. A., & Kiørboe, T. (2008). Maximum phytoplankton concentrations in the sea. *Limnology and Oceanography*, *53*(1), 395–399. https://doi.org/10.4319/lo.2008.53.1.0395

Jakobsen, H. H., & Markager, S. (2016). Carbon-to-chlorophyll ratio for phytoplankton in temperate coastal waters: Seasonal patterns and relationship to nutrients. *Limnology and Oceanography*, *61*(5), 1853–1868. https://doi.org/10.1002/lno.10338

Jassby, A. D., & Platt, T. (1976). Mathematical formulation of the relationship between photosynthesis and light for phytoplankton. *Limnology and Oceanography*, *21*(4), 540–547. https://doi.org/10.4319/lo.1976.21.4.0540

Johnson, K. S., Gordon, R. M., & Coale, K. H. (1997). What controls dissolved iron concentrations in the world ocean? *Marine Chemistry*, *57*(3-4), 137–161. https://doi.org/10.1016/S0304-4203(97)00043-1

Karp, N. A., Segonds-Pichon, A., Gerdin, A. K., Ramírez-Solis, R., & White, J. K. (2012). The fallacy of ratio correction to address confounding factors. *Laboratory Animals*, *46*(3), 245–252. https://doi.org/10.1258/la.2012.012003

Klaas, C., & Archer, D. E. (2002). Association of sinking organic matter with various types of mineral ballast in the deep sea: Implications for the rain ratio. *Global Biogeochemical Cycles*, *16*(4), 1116. https://doi.org/10.1029/2001GB001765

Laurenceau-Cornec, E. C., Trull, T. W., Davies, D. M., Bray, S. G., Doran, J., Planchon, F., Carlotti, F., et al. (2015). The relative importance of phytoplankton aggregates and zooplankton fecal pellets to carbon export: Insights from free-drifting sediment trap deployments in naturally iron-fertilised waters near the Kerguelen Plateau. *Biogeosciences*, *12*(4), 1007–1027. https://doi.org/10.5194/bg-12-1007-2015

Laws, E. A., D'Sa, E., & Naik, P. (2011). Simple equations to estimate ratios of new or export production to total production from satellite-derived estimates of sea surface temperature and primary production. *Limnology and Oceanography: Methods*, *9*(12), 593–601. https://doi.org/10.4319/lom.2011.9.593

Laws, E. A., Falkowski, P. G., Smith, W. O., Ducklow, H., & McCarthy, J. J. (2000). Temperature effects on export production in the open ocean. *Global Biogeochemical Cycles*, *14*(4), 1231–1246. https://doi.org/10.1029/1999GB001229

Laws, E. A., Letelier, R. M., & Karl, D. M. (2014). Estimating the compensation irradiance in the ocean: The importance of accounting for non-photosynthetic uptake of inorganic carbon. *Deep Sea Research I*, *93*, 35–40. https://doi.org/10.1016/j.dsr.2014.07.011

Le Moigne, F. A. C., Henson, S. A., Cavan, E., Georges, C., Pabortsava, K., Achterberg, E. P., Ceballos-Romero, E., et al. (2016). What causes the inverse relationship between primary production and export efficiency in the Southern Ocean? *Geophysical Research Letters*, *43*, 4457–4466. https://doi.org/10.1002/2016GL068480

Letelier, R. M., Karl, D. M., Abbott, M. R., & Bidigare, R. R. (2004). Light driven seasonal patterns of chlorophyll and nitrate in the lower euphotic zone of the North Pacific Subtropical Gyre. *Limnology and Oceanography*, *49*(2), 508–519. https://doi.org/10.4319/lo.2004.49.2.0508

Li, Z. (2017). Remotely sensed estimates and controls of large-scale oceanic net community production, PhD dissertation, Duke University, ProQuest Dissertations Publishing, 10258797.

Li, Z., & Cassar, N. (2016). Satellite estimates of net community production based on O_2/Ar observations and comparison to other estimates. *Global Biogeochemical Cycles*, *30*, 735–752. https://doi.org/10.1002/2015GB005314

Li, Z., & Cassar, N. (2017). A mechanistic model of an upper bound on oceanic carbon export as a function of mixed layer depth and temperature. *Biogeosciences*, *14*(22), 5015–5027. https://doi.org/10.5194/bg-14-5015-2017

Lima, I. D., Lam, P. J., & Doney, S. C. (2014). Dynamics of particulate organic carbon flux in a global ocean model. *Biogeosciences*, *11*(4), 1177–1198. https://doi.org/10.5194/bg-11-1177-2014

Lopez-Urrutia, A., San Martin, E., Harris, R. P., & Irigoien, X. (2006). Scaling the metabolic balance of the oceans. *Proceedings of the National Academy of Sciences of the United States of America*, *103*(23), 8739–8744. https://doi.org/10.1073/pnas.0601137103

Lorenzen, C. J. (1976). Primary production in the sea. In D. H. Cushing & J. J. Walsh (Eds.), *Ecology of the seas* (pp. 173–185). Oxford: Blackwell scientific publications.

Lutz, M., Dunbar, R., & Caldeira, K. (2002). Regional variability in the vertical flux of particulate organic carbon in the ocean interior. *Global Biogeochemical Cycles*, *16*(3), 1037. https://doi.org/10.1029/2000GB001383

Maiti, K., Charette, M. A., Buesseler, K. O., & Kahru, M. (2013). An inverse relationship between production and export efficiency in the Southern Ocean. *Geophysical Research Letters*, *40*, 1557–1561. https://doi.org/10.1002/grl.50219

Marra, J. F., Lance, V. P., Vaillancourt, R. D., & Hargreaves, B. R. (2014). Resolving the ocean's euphotic zone. *Deep Sea Research Part I: Oceanographic Research Papers*, *83*, 45–50. https://doi.org/10.1016/j.dsr.2013.09.005

Martin, J. H., Gordon, R. M., & Fitzwater, S. E. (1990). Iron in Antarctic waters. *Nature*, *345*(6271), 156–158. https://doi.org/10.1038/345156a0

Martin, J. H., Knauer, G. A., Karl, D. M., & Broenkow, W. W. (1987). Vertex—Carbon cycling in the Northeast Pacific. *Deep Sea Research*, *34*(2), 267–285. https://doi.org/10.1016/0198-0149(87)90086-0

Michaels, A. F., & Silver, M. W. (1988). Primary production, sinking fluxes and the microbial food web. *Deep Sea Research*, *35*(4), 473–490. https://doi.org/10.1016/0198-0149(88)90126-4

Mitchell, B. G., Brody, E. A., Holm-Hansen, O., Mcclain, C., & Bishop, J. (1991). Light limitation of phytoplankton biomass and macronutrient utilization in the Southern Ocean. *Limnology and Oceanography*, *36*(8), 1662–1677. https://doi.org/10.4319/lo.1991.36.8.1662

Mitchell, B. G., & Holm-Hansen, O. (1991). Observations and modeling of the Antarctic phytoplankton crop in relation to mixing depth. *Deep Sea Research*, *38*(8–9), 981–1007. https://doi.org/10.1016/0198-0149(91)90093-U

Moore, C. M., Mills, M. M., Arrigo, K. R., Berman-Frank, I., Bopp, L., Boyd, P. W., Galbraith, E. D., et al. (2013). Processes and patterns of oceanic nutrient limitation. *Nature Geoscience*, *6*(9), 701–710. https://doi.org/10.1038/ngeo1765

Morel, A., Huot, Y., Gentili, B., Werdell, P. J., Hooker, S. B., & Franz, B. A. (2007). Examining the consistency of products derived from various ocean sensors in open ocean (Case 1) waters in the perspective of a multi-sensor approach. *Remote Sensing of Environment*, *111*(1), 69–88. https://doi.org/10.1016/j.rse.2007.03.012

Moreno, A. R., & Martiny, A. C. (2018). Ecological stoichiometry of ocean plankton. *Annual Review of Marine Science*, *10*(1), 43–69. https://doi.org/10.1146/annurev-marine-121916-063126

Murray, J. W., Young, J., Newton, J., Dunne, J., Chapin, T., Paul, B., & McCarthy, J. J. (1996). Export flux of particulate organic carbon from the central equatorial Pacific determined using a combined drifting trap-^{234}Th approach. *Deep Sea Research, Part II*, *43*(4-6), 1095–1132. https://doi.org/10.1016/0967-0645(96)00036-7

Nelson, D. M., & Smith, W. O. (1991). Sverdrup revisited: Critical depths, maximum chlorophyll levels, and the control of Southern Ocean productivity by the irradiance-mixing regime. *Limnology and Oceanography*, *36*(8), 1650–1661. https://doi.org/10.4319/lo.1991.36.8.1650

Pahlow, M., & Oschlies, A. (2009). Chain model of phytoplankton P, N and light colimitation. *Marine Ecology Progress Series*, *376*, 69–83. https://doi.org/10.3354/meps07748

Palevsky, H. I., & Doney, S. C. (2018). How choice of depth horizon influences the estimated spatial patterns and global magnitude of ocean carbon export flux. *Geophysical Research Letters*, *45*, 4171–4179. https://doi.org/10.1029/2017GL076498

Passow, U., Alldredge, A. L., & Logan, B. E. (1994). The role of particulate carbohydrate exudates in the flocculation of diatom blooms. *Deep-Sea Research Part I*, *41*(2), 335–357. https://doi.org/10.1016/0967-0637(94)90007-8

Rivkin, R. B., & Legendre, L. (2001). Biogenic carbon cycling in the upper ocean: Effects of microbial respiration. *Science*, *291*(5512), 2398–2400. https://doi.org/10.1126/science.291.5512.2398

Sarmiento, J. L., & Gruber, N. (2006). *Ocean biogeochemical dynamics*. Princeton, NJ: Princeton Univ. Press.

Sathyendranath, S., Stuart, V., Cota, G., Mass, H., & Platt, T. (2001). Remote sensing of phytoplankton pigments: A comparison of empirical and theoretical approaches. *International Journal of Remote Sensing*, *22*(2-3), 249–273. https://doi.org/10.1080/014311601449925

Siegel, D. A., Buesseler, K. O., Doney, S. C., Sailley, S. F., Behrenfeld, M. J., & Boyd, P. W. (2014). Global assessment of ocean carbon export by combining satellite observations and food-web models. *Global Biogeochemical Cycles*, *28*, 181–196. https://doi.org/10.1002/2013GB004743

Smith, S. L., Yamanaka, Y., Pahlow, M., & Oschlies, A. (2009). Optimal uptake kinetics: Physiological acclimation explains the pattern of nitrate uptake by phytoplankton in the ocean. *Marine Ecology Progress Series*, *384*, 1–12. https://doi.org/10.3354/meps08022

Thornton, D. C. O. (2014). Dissolved organic matter (DOM) release by phytoplankton in the contemporary and future ocean. *European Journal of Phycology*, *49*(1), 20–46. https://doi.org/10.1080/09670262.2013.875596